

Ionic wind produced by a millimeter-gap DC corona discharge ignited between a plate and an inclined needle

Eric Moreau*, Sonia Souakri, Romain Bellanger, Nicolas Benard

University of Poitiers, PPRIME Institute (CNRS, ISAE-ENSMA), Téléport2, BP30179, 86962 Futuroscope, France

* Corresponding author: eric.moreau@univ-poitiers.fr (Eric Moreau)

Received: 13 June 2020

Revised: 10 December 2020

Accepted: 9 January 2021

Published online: 27 January 2021

Abstract

This study aims at characterizing the ionic wind produced by a DC corona discharge ignited between a high voltage needle and a grounded plate electrode. The influence of several input parameters is investigated: the value and polarity of the applied voltage, the electrode gap (2.5 and 5 mm) and the angle between the plate and the needle (30°, 45° and 90°). The main results are as follows: (a) the positive corona discharge generates a higher ionic wind velocity compared to the negative one but a smaller flow rate because the produced jet is thinner, (b) the topology of the produced jet flow depends on the value and the polarity of the applied voltage, and it is linked to the discharge regime, (c) when the needle is perpendicular to the plate, the ionic wind jet impacts the plate in front of the needle, (d) when the needle is inclined, the angle of the ionic wind jet is weakly higher than the one of the needle, (e) in fact, the ionic wind jet follows the electric field lines close to the tip but it is deviated from its initial trajectory when one moves away from the tip, (f) downstream of the location at which the main jet impacts the plate wall, the ionic wind direction becomes parallel to the wall, (g) the velocity of this wall jet is maximum when we used a positive voltage, and the smallest gap and needle angle (2.5 mm and 30°, respectively in this study), (h) we can expect to enhance the wall jet performance by decreasing these both values in the future and that is encouraging to perfect new types of plasma actuators for applications such as airflow control or thermal exchange enhancement.

Keywords: Corona discharge, inclined needle, ionic wind, electrohydrodynamics, wall jet.

1. Introduction

The ionic wind is an electrohydrodynamic (EHD) phenomenon that is known to be due to the drift of electric charges within a corona discharge. This phenomenon has been the subject of numerous research mainly due to its many applications, such as fluid pumping [1–6], air cleaning [7–11], evaporation and drying [12–14], cooling [15, 16], heat transfer [17–19], surface treatment [20], airflow control [21, 22] and EHD thruster [23–25] for instance. However, although several recent papers aimed at better understanding the precise origin of ionic wind and the interactions between the plasma discharge and the surrounding gas [26–30], the underlying physical mechanisms are not precisely known. As notified by Fylladitakis *et al* [31], the first observation and record of EHD phenomena started with Niccolo Cabeo who noticed in 1629 the attraction, the contact and finally the repulsion of sawdust by electrified body, even if he did not link it to this effect [32]. Officially, the discovery of electrohydrodynamics in gas was attributed to Hauksbee for his work in 1709. Since numerous scientists have been working on this subject, such as Newton [33] who continued work of Hauksbee and gave the name of “electric wind”. Finally, Chattok [34] published the first article about EHD phenomena produced by corona discharges in atmospheric air.

In the present experimental study, we aim at characterizing the electrohydrodynamic phenomena and the resulting ionic wind induced within DC positive and negative corona discharges in atmospheric air, with a non-usual geometry: a small gap between both electrodes (down to 2.5 mm) and a needle which is not

perpendicular to the plate electrode. When this experimental work has been carried out, only one study on the ionic wind produced by a positive corona discharge in this type of geometrical configuration had been published [35]. The same research team published a second article on this subject very recently [36]. To our knowledge, these are the only two publications dealing with the ionic wind produced by a corona discharge with a needle which is not perpendicular to the plate although this configuration has many interests. The first one is a scientific interest; in modifying the electrode geometry, we modify the spatial distribution of the space charge between both electrodes and we can expect to better understand the electrohydrodynamic phenomena that take place inside the discharge. The second interest is linked to the applications of such a discharge. Indeed, when the needle is not perpendicular to the plate electrode, the ionic jet topology is fully different. In fact, we will see in this paper that the jet is composed of two parts. The first part corresponds to the primary jet starting from the needle and flowing toward the plate; we will be able to observe that its topology is close to the one of a typical needle-to-plate design when the needle is perpendicular to the plate, excepted that its angle is governed by the needle angle. The second part is the flow downstream the stagnation point, i.e. the location where the primary jet impacts the plate. In this region, the jet becomes parallel to the plate wall, as it is the case for typical plasma actuators based on surface corona discharges or surface dielectric barrier discharges [21]. Both parts of the ionic wind jet are of significant interest for plasma actuators; the primary jet induces a suction effect toward the wall and the second part of the jet results in air acceleration close to the wall. In practice, these both phenomena could be used for flow separation control in aerodynamics or to enhance the thermal exchanges between air and a solid wall.

The present paper will be divided in several parts. First, we will present the I-V curve of both positive and negative corona discharges. Secondly, we will study the ionic wind produced by a typical needle-to-plate corona discharge, with a gap equal to 5 mm. Third, we will incline the needle at 45 degrees and we will characterize the produced ionic wind for two gaps, 5 mm and 2.5 mm. This configuration is original and singular as the needle is inclined and the gap is very small compared to usual. Then, we will decrease the angle at 30 degrees, still with a gap of 2.5 mm. Finally, we will focus on the second part of the ionic wind jet (downstream the stagnation point) for all these geometrical cases.

2. Experimental setup

The experimental setup consists of a tungsten needle with a length of 38 mm, a diameter equal to 0.51 mm and a tip with a curvature radius equal to 100 μm (PTG20-100.0/microworld.eu). The collecting electrode is a stainless steel rectangular plate with rounded edges. Its size is equal to $269 \times 217 \text{ mm}^2$ and its thickness is 4 mm. The plate is placed horizontally. The system allows us to independently modify the distance between the electrodes and the angle between them (Fig. 1a). A high voltage (HV) amplifier (Trek, 30 kV, 20 mA) generates the high DC voltage applied at the needle. Moreover, a resistance of 500 k Ω is placed between the HV power supply and the needle. In order to plot the current-voltage characteristics of the corona discharge, a resistor of 10 k Ω is added between the plate and earth. First, a positive voltage ramp is applied between both electrode from 0 to +6 kV during 10 seconds and the time-averaged current is measured across the 10 k Ω resistor every 10 milliseconds during 10 ms with the help of an oscilloscope (Lecroy 24Xs-A, 200MHz, sampling rate set to 1 Gs s⁻¹). To plot the I-V curve of the negative corona discharge, the same protocol is used, but with a negative voltage ramp, from 0 to -6 kV.

To determine the ionic wind velocity, a Particle Image Velocimetry (PIV) system is used. For that, the point-to-plate design is placed in a glass tank in which seeding particles are injected. An atomizer (Topas ATM 210) is used to produce 0.5 μm -diameter oil droplets (Ondina). Moreover, a laser sheet lightens the field of view and the seeding particle motion is visualized with a CCD camera. More precisely, a solid-state laser system (Nd-YAG – Laser Quantel Twins Ultra 30 mJ from Big Sky Laser) produces a laser sheet with a wavelength of 532 nm and a thickness of about 0.5 mm. This laser sheet illuminates the seeding particles entrained by the ionic wind in the region between the needle and the plate. A high-resolution camera (LaVision LX16M Camlink with a CCD sensor of $27 \times 18 \text{ mm}^2$ and 4920×3280 pixels) allows us to record successive pairs of images of the particle motion (500 to 2500 non-correlated images are recorded depending on the case). However, as it can be seen in Figure 1b, the convergence of the mean ionic wind velocity is obtained from about 500 images. The image acquisition frequency is set to 8.24 Hz, with a time delay from 6 μs to 20 μs between two consecutive images of one single pair. This time delay is adjusted to maintain the particle displacement in a range of around 8 pixels. Both velocity components are computed using a cross correlation

algorithm (Davis software) with adaptive multipasses and a decreasing interrogation window of 64×64 down to 16×16 pixels and an overlap set to 50%. The spatial resolution of the resulting velocity vector fields corresponds to one vector every $17 \mu\text{m}$.

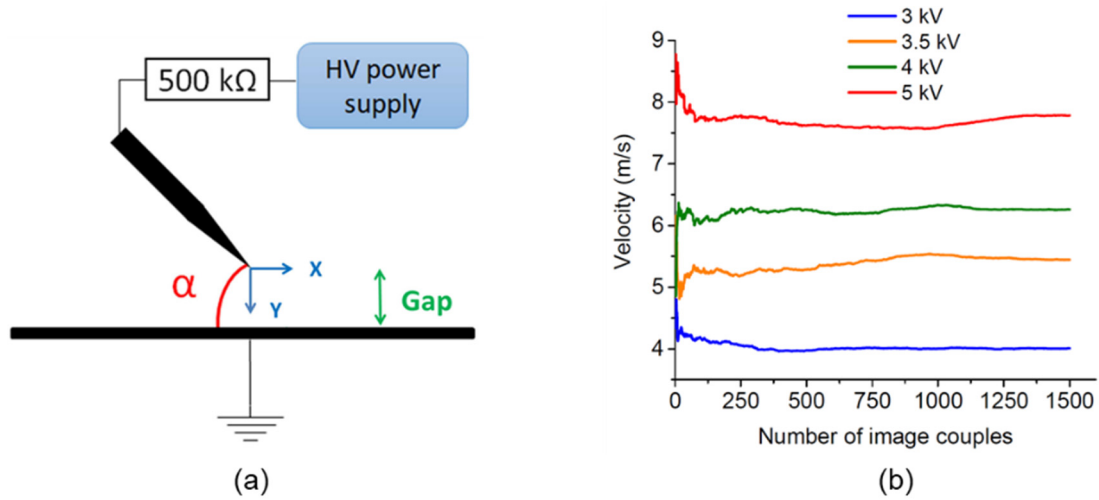


Fig. 1. (a) Experimental setup of the corona discharge: needle-to-plate geometry with adjustable gap (g) and angle of the needle compared the plate (α); (b) Convergence of the ionic wind velocity. The studied case is as follows: gap $g = 2.5 \text{ mm}$, angle between both electrodes $\alpha = 45^\circ$, location of the velocity measurement $y = 1.25 \text{ mm}$ (middistance between both electrodes).

3. Results and discussion

3.1 Electrical measurements and potential charge of seeding particles

Fig. 2 presents the I-V characteristics of positive and negative corona discharges, in presence and in absence of oil seeding particles and for a gap of 5 mm. Several main remarks can be made. First, in the case of the positive discharge, we can see that the discharge starts to ignite at +2.9 kV whatever the conditions are ($\alpha = 90^\circ$, $\alpha = 45^\circ$, with/without particles) and then increases up to 5 about $14 \mu\text{A}$ at +6 kV. The first interesting remark is that the angle of the needle and the presence or not of particles does not affect significantly the discharge current. That highlights more especially that the seeding particles do not charge and we can then assume that their motion is mainly due to the ionic wind and not to the phenomenon of electrostatic precipitation. Indeed, when the particles are charged, such as in an electrostatic precipitator, the current in presence of particles is different to the one measured in absence of particles because a part of the total current is due to the collection of charged particles. For instance, Zouzou *et al* [37] highlighted that the presence of incense smoke particles in DC positive and negative point-to-plate corona discharges resulted in a significant decrease of the time-averaged current as the particles moved slower than ions. In the same way, Dramane *et al* [9] observed a decrease of the current and the power consumption of a dielectric barrier discharge reactor in presence of the same particles. Furthermore, two recent articles demonstrated that the motion of the oil droplets used as seeding particles in the present study was due to ionic wind and not the fact that these particles could be charged and then submitted to Coulomb force [38, 39]. Indeed, in the one hand, Defoort *et al* [38], as previously in the article of Akishev *et al* [40], demonstrated that the motion of water droplets in a positive corona discharge was not due only to ionic wind but also to electrostatic precipitation, resulting in a slipping between the airflow and the water droplets. On the other hand, they highlighted that the oil droplets followed perfectly the ionic wind. Moreover, Moreau and Benard [39] and Moreau *et al* [27] characterized the ionic wind produced by a positive corona discharge with two different systems: a particle image velocimetry one and a second one that does not require seeding particles (Schlieren bench). In this study, they highlighted that both measurements resulted in the same qualitative result. Finally, to confirm that the phenomenon of electrostatic precipitation is negligible, we can indicate that there was no oil deposition on the grounded plate even when the experiments were very long.

In the case of the negative discharge, the behaviour is different. First, the current of the negative discharge is globally about three times higher than the one of the positive discharges. Moreover, the I-V curve changes when the needle angle is modified and when seeding particles are added to the quiescent air, especially around the ignition voltage. For $\alpha = 90$ degrees, the current suddenly increases up to $6 \mu\text{A}$ at $V = 3.5 \text{ kV}$ (in practise, the voltage and the current are negative). For $\alpha = 45$ degrees, the current starts to increase at $V = 3.1 \text{ kV}$ and reaches $3.7 \mu\text{A}$ at $V = 3.3 \text{ kV}$. Finally, when there are seeding particles, the current increases gradually, as for the positive corona discharge, from $V = 2.6 \text{ kV}$. In fact, one can say that the I-V curve is modified only between 2.6 kV and 3.5 kV , when the discharge starts to ignite. That highlights that some particles are electrically charged in this voltage range and are submitted to the phenomenon of electrostatic precipitation. In the other hand, for voltages higher than 3.5 kV , the three curves are similar. For this reason, for a gap equal to 5 mm , no ionic wind measurements for voltages smaller than 3.5 kV will be presented.

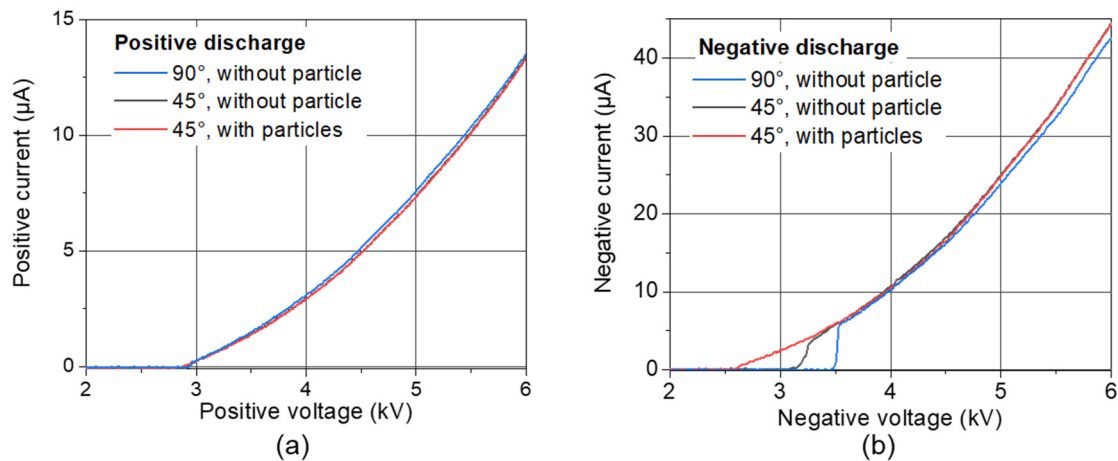


Fig. 2. Current-voltage characteristics of positive and negative corona discharges in absence and in presence of seeding particles for needle angles equal to 90° and 45° .

3.2 Ionic wind velocity with a vertical needle

The first set of experiments is realized with an usual typical configuration: the tip is perpendicular to the plate, i.e. the angle α is equal to 90° . The electrode gap is equal to 5 mm . The tip of the needle is located at $x = 0 \text{ mm}$ and $y = 0 \text{ mm}$, and the plate is placed at $y = 5 \text{ mm}$. Fig.3 presents the time-averaged velocity fields obtained for different positive and negative voltages. The background colour corresponds to the velocity norm and the flow streamlines reveal the jet topology. First, one can see that an ionic wind jet starts from the high voltage needle and moves towards the grounded plate electrode. The jet topology is similar to fluidic system with three main regions. First, a free jet region is formed where the flow is not influenced by the confinement induced by the plate. In this first region, the velocity is mainly axial. On the border of the jet, shear layers develop because of the inflectional velocity profile across jet section. When the jet impacts the flat plate, the flow is deflected and a stagnation region is formed. Finally, boundary layers develop along the flat plate wall. Although the ionic wind jet versus time is prone to move from left to right when it impacts the plate (this is not visible here but this “flapping” phenomenon is sometimes present in the case of fluidic impacting jets), one can observe that the time-averaged jet remains perpendicular to the plate. This remark is not fortuitous, as it is sometimes complicated to obtain such a stable jet. Secondly, it appears that the produced ionic wind depends strongly on the voltage polarity. For a negative discharge, the ionic wind jet is wider than for the positive discharge, but its velocity is smaller, as previously observed by Moreau *et al* [26] with an electrode gap of 25 mm and Defoort *et al* [30] for a gap equal to 15 mm . Indeed, we know that positive corona discharges produce usually a faster jet but its velocity versus time fluctuates more than the one of negative coronas.

In order to compare more accurately the differences between both polarities, we plotted velocity profiles from the PIV velocity fields (along x axis), midway between both electrodes at $y = 2.5 \text{ mm}$ (Figure 4). With these profiles, we can clearly see that the positive ionic wind mean velocity is higher than the negative one. It is especially visible in front of the needle that corresponds to the center of the jet. For instance, at the same absolute voltage value $|V| = 5 \text{ kV}$, the ionic wind reaches 7.2 m s^{-1} with the positive corona when it is limited to 5.2 m s^{-1} with the negative corona since the positive current is equal to $7.5 \mu\text{A}$ and the negative one to 25

μA . That shows that the positive discharge produces a faster ionic wind with a weaker current, highlighting that the electro-mechanical efficiency of a positive discharge is higher than the one of the negative discharge, as already demonstrated by Moreau and Touchard [1] in the case of point-to-grid coronas. However, we can also remark that the positive ionic wind is higher only for $|V| \geq 4 \text{ kV}$ because at $|V| = 3.5 \text{ kV}$, the positive discharge induces a very weak ionic wind, certainly because the discharge is just ignited and a streamer-free regime occurs (the mean current is very low and equal to $1.4 \mu\text{A}$).

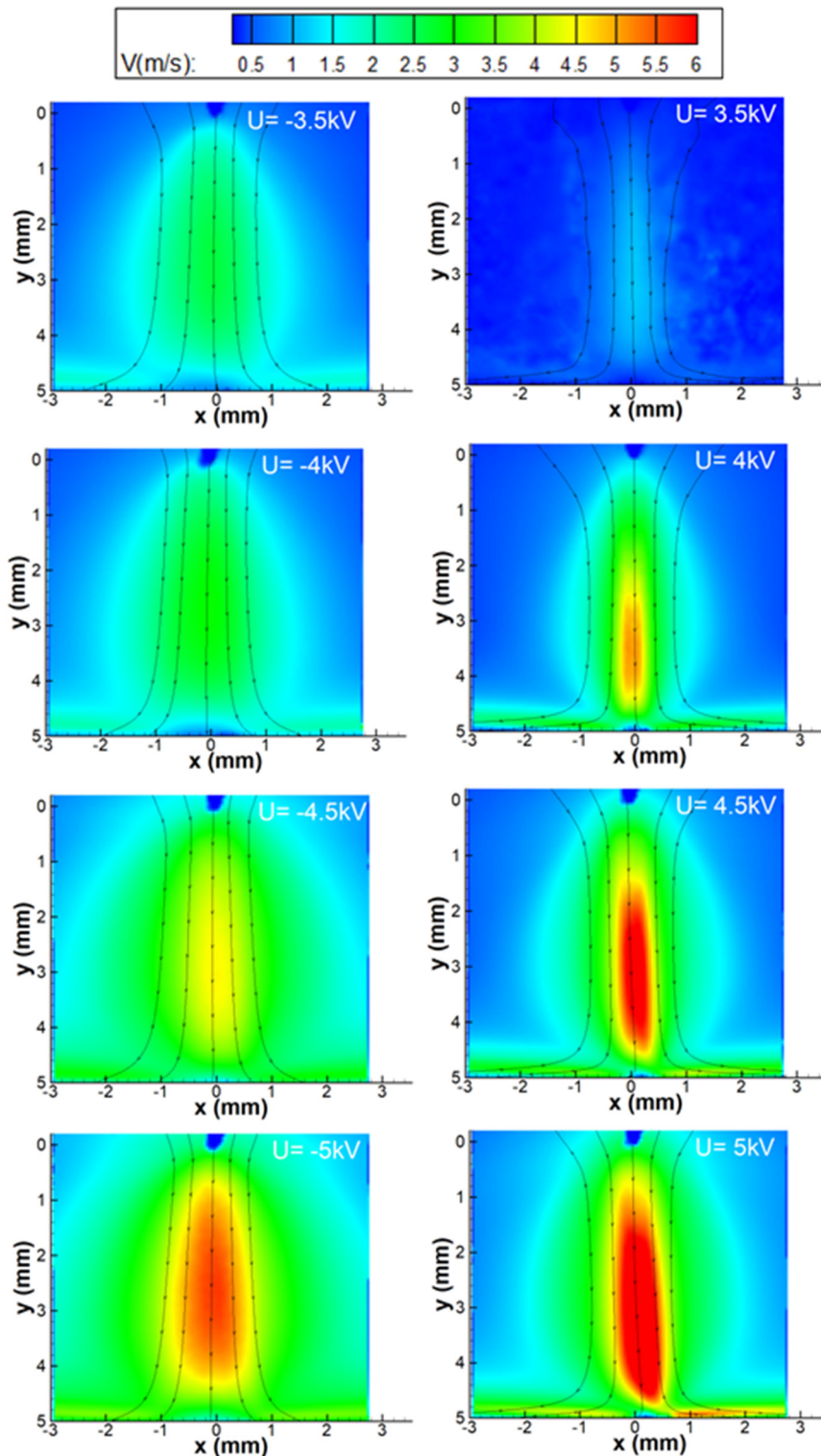


Fig. 3. Velocity fields with streamlines of the ionic wind produced by a negative (a) and positive (b) point-to-plate corona discharge for several voltage values ($\alpha = 90^\circ$ and gap = 5 mm).

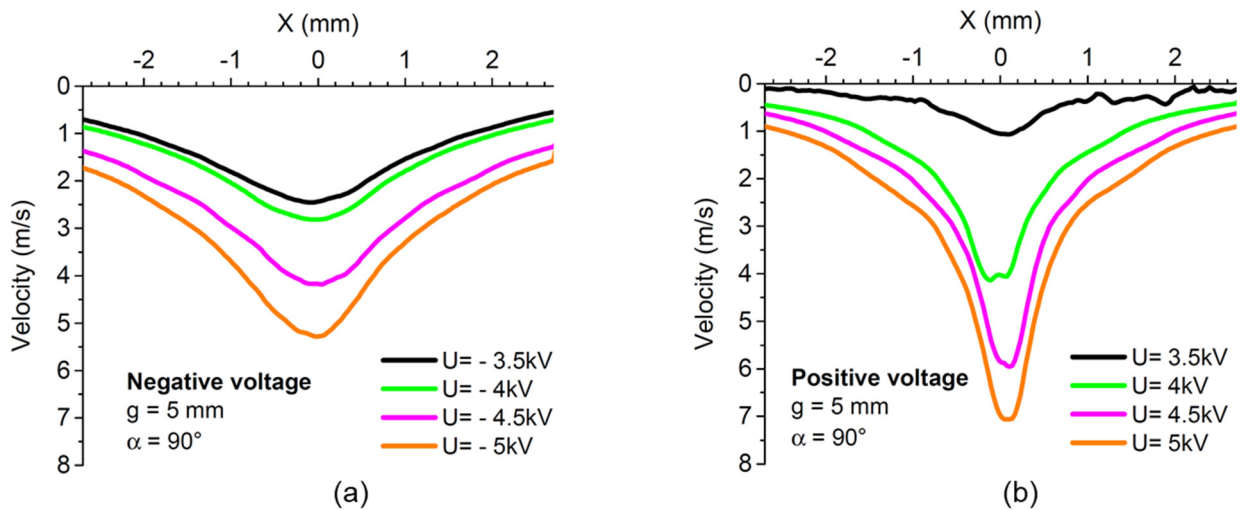


Fig. 4. Velocity profiles along the x axis at $y = 2.5$ mm (mid-distance between both electrodes) for a negative (a) and a positive (b) corona discharge.

Fig. 5 presents velocity profiles extracted from the PIV velocity fields along the y axis, in front of the tip (at $x = 0$). In the case of a negative corona (Figure 5a), the velocity increases from the needle ($x = 0$) and reaches its maximum value at $y \approx 2.5$ mm. Then velocity starts to decrease and is equal to zero at the wall where the jet impact the plate ($y = 5$ mm). For the positive corona (Figure 5b), the velocity profiles are different; the velocity is higher and its maximum value is obtained further from the tip, at $y \approx 3$ mm. The dissimilarity between both polarities is due to a different space charge distribution in the inter-electrode region, and to different discharge regimes. For instance, we can assume that the presence of streamers in positive coronas and Trichel pulses in negative coronas influence the dynamics and the time-averaged characteristics of the flow, as it has been recently highlighted by Moreau *et al* [27] and Mizeraczyk *et al* [29]. However, we cannot confirm the link between the electrical and the mechanical characteristics of the discharge because the current versus time has not been measured during the PIV measurements.

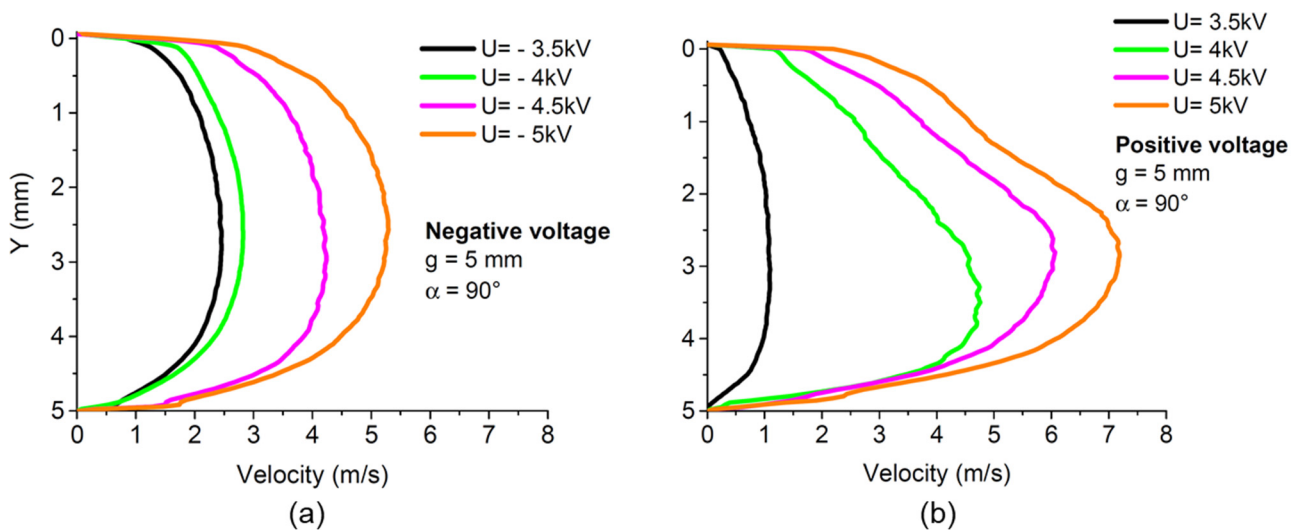


Fig. 5. Velocity profiles along the Y-axis for negative (a) and positive (b) corona discharges at $x = 0$ mm).

By integrating the velocity profiles of Fig. 5(a), we obtain the surface flow rate (Table 1). Although this computation is incomplete because it is computed only for $x \in [-2.7; 2.7]$ and it is not the true flow rate in $\text{m}^3 \text{s}^{-1}$, it gives a relevant information and tendency: the flow rate is higher in the case of the negative corona. Indeed, with the negative discharge, the ionic wind velocity is smaller but the jet is wider, resulting in a higher flow rate. Therefore, if the aim is to produce a high flow rate, as in ion-pumps [2], it is preferable to use a negative discharge.

Table 1. Flow rate of the ionic wind for negative and positive corona discharges ($\alpha = 90^\circ$ and gap = 5 mm).

Negative voltage (kV)	Surface flow rate ($10^{-3} \text{ m}^2 \text{ s}^{-1}$)	Positive voltage (kV)	Surface flow rate ($10^{-3} \text{ m}^2 \text{ s}^{-1}$)
-3.5	7.93	3.5	2.10
-4.0	9.19	4.0	8.08
-4.5	13.90	4.5	11.32
-5.0	17.22	5.0	14.17

3.3 Ionic wind velocity with an inclined needle

Now, the needle is inclined at an angle with the plate equal to $\alpha = 45^\circ$. With this angle, two electrode gaps have been studied: 5 mm and 2.5 mm.

3.3.1 Ionic wind jet for a gap = 5 mm and $\alpha = 45^\circ$

We started our experiments with a gap equal to 5 mm. The velocity fields are presented in Fig. 6. Several remarks can be done. On the one hand, the jet is no longer perpendicular to the plate wall. Indeed, as observed in a previous study of Elagin *et al* [35] in the case of a positive corona, the angle jet close to the tip follows the needle angle, meaning that the jet is aligned with the needle. This is due to the fact that the ionic wind topology is governed by the electric field lines which are parallel to the needle when we are close to the tip.

On the other hand, the jet impacts the plate wall at $x \approx 3$ mm and $x \approx 4$ mm for the negative and positive coronas, respectively. That means that the angle of the whole jet compared to the plate is not equal exactly to 45° (in this case, the impact would occur at $x = 5$ mm) and differs according to the voltage polarity; it is equal to 59° and 52° for the negative and positive discharges, respectively. Elagin *et al* [35] found also a jet angle slightly higher than the needle one. Moreover, one can see that the ionic wind velocity is higher in the case of the positive discharge, as in the case $\alpha = 90^\circ$. By the way, that is confirmed by the velocity profiles at $y = 2.5$ mm (Fig. 7).

That is certainly one of the reasons why the angle of the positive jet is closer to the one of the needle. However, one can think that there are also physical reasons, like the presence of streamers that do not follow the electric field lines and are known to be parallel to the needle. Finally, downstream the location where the jet impacts the wall ($x > 5$ mm), the jet becomes parallel to the wall. The jet downstream the impact location will be more precisely studied at the end of this article.

3.3.2 Ionic wind jet for a gap = 2.5 mm and $\alpha = 45^\circ$

Fig. 8 presents the same experiments, but with a gap equal to 2.5 mm and a positive high voltage. We can see one more time that an inclined jet is produced, but with a higher velocity. Indeed, when the gap is reduced to 2.5 mm, the maximal ionic wind velocity reaches 8 m s^{-1} at 5 kV (Fig. 9). Here again, the jet angle is not equal to the needle one. Considering an impact location at $x \approx 1.6$ mm, the jet angle can be estimated to about 57° . Fig. 10 illustrates the peak value of the velocity norm (V_M) and the flow rate versus applied voltage for a gap of 5 mm and 2.5 mm, the maximum velocity values being obtained from the previous velocity profiles. First, we can observe that in this voltage range, the norm of the velocity increases approximately linearly with the high voltage, whatever the voltage polarity and electrode gap are. This result is not surprising since it has been verified several times theoretically and experimentally by several studies, such as the one of Robinson [2] in 1961 and other ones more recently [28, 41]. Secondly, the ionic wind velocity depends on these both input parameters. At ± 3.5 kV and with a gap of 5 mm, V_M is equal to 2.8 m s^{-1} and 3.8 m s^{-1} for the negative and positive discharges, respectively. For the same applied voltage and with a gap of 2.5 mm, $V_M = 5.9 \text{ m s}^{-1}$. Let us take another example: with a gap of 2.5 mm, $V_M = 5.25 \text{ m s}^{-1}$ for 3.25 kV. To reach the same velocity value with a gap of 5 mm, voltages of +4.25 kV or -5.1 kV are necessary. From Fig. 10b, it can be stated that the case resulting in the lowest maximal velocity does not lead to the lowest surface flow. For instance, with the 5-mm gap negative corona, the maximal velocity is the weakest, but the value of the surface flow rate is comparable to the case of a positive corona with a gap of 2.5 mm (higher maximal velocity). This point is interesting because this brings us to two conclusions. First, if we want to produce a maximum velocity, we

should use a positive high voltage with a small gap between both electrodes. On the contrary, to generate a maximum flow rate, it is more relevant to use a negative high voltage.

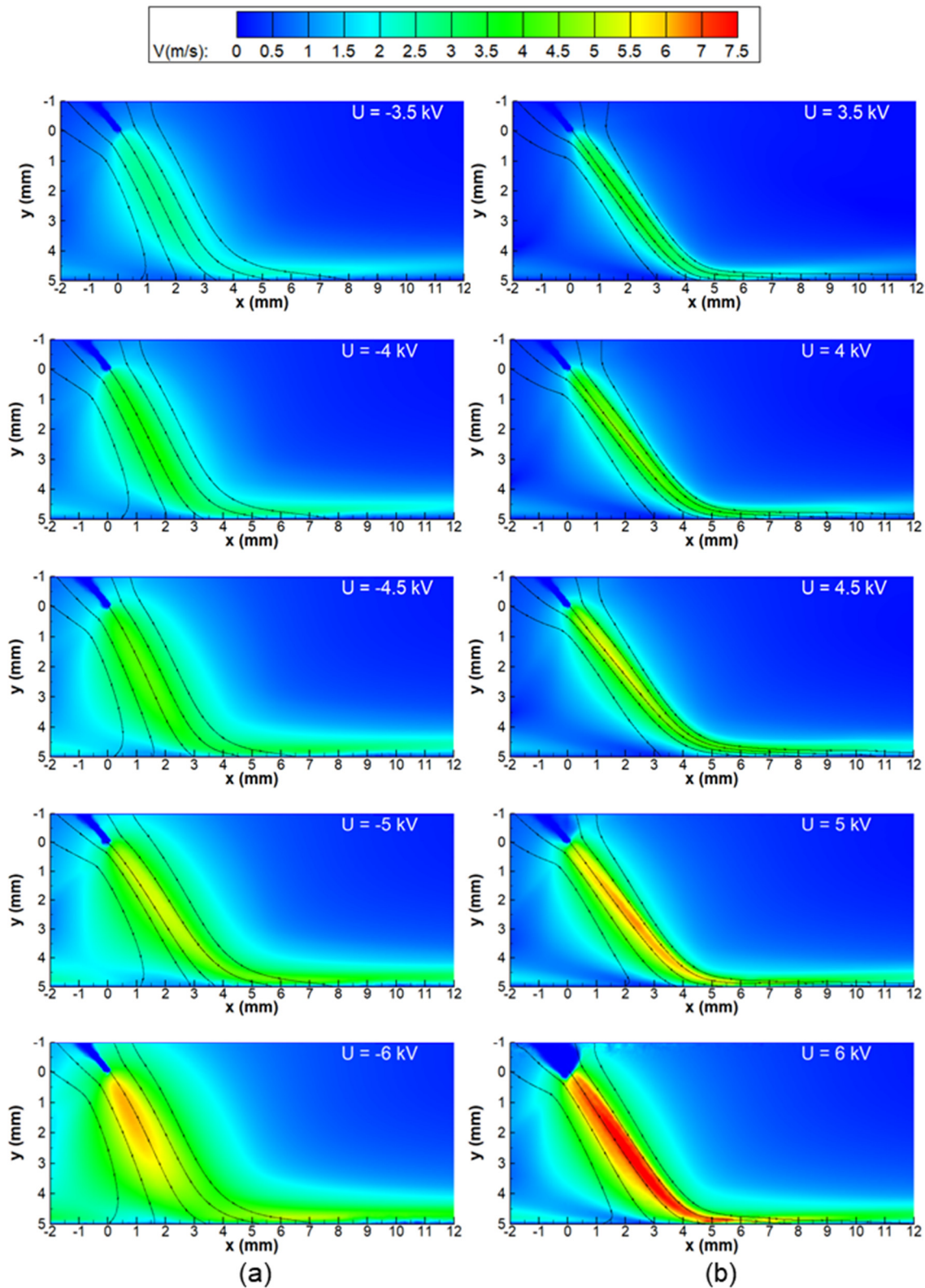


Fig. 6. Velocity fields and with streamlines of the ionic wind jet produced by a point-to-plate negative (a, left column) and positive (b, right column) corona discharges with a needle inclined at 45° compared to the plate and a gap of 5 mm. The tip is located at (0,0) and the plate at $y = 5$ mm.

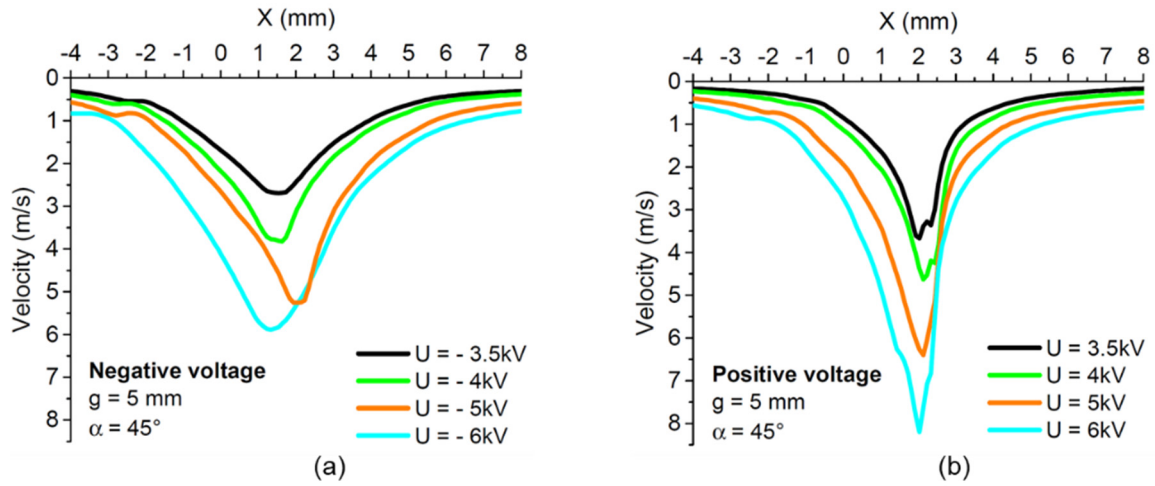


Fig. 7. Velocity profiles along X axis at $y = 2.5$ mm (midway both electrodes) for the negative (a) and positive (b) corona discharges (gap = 5 mm and $\alpha = 45^\circ$).

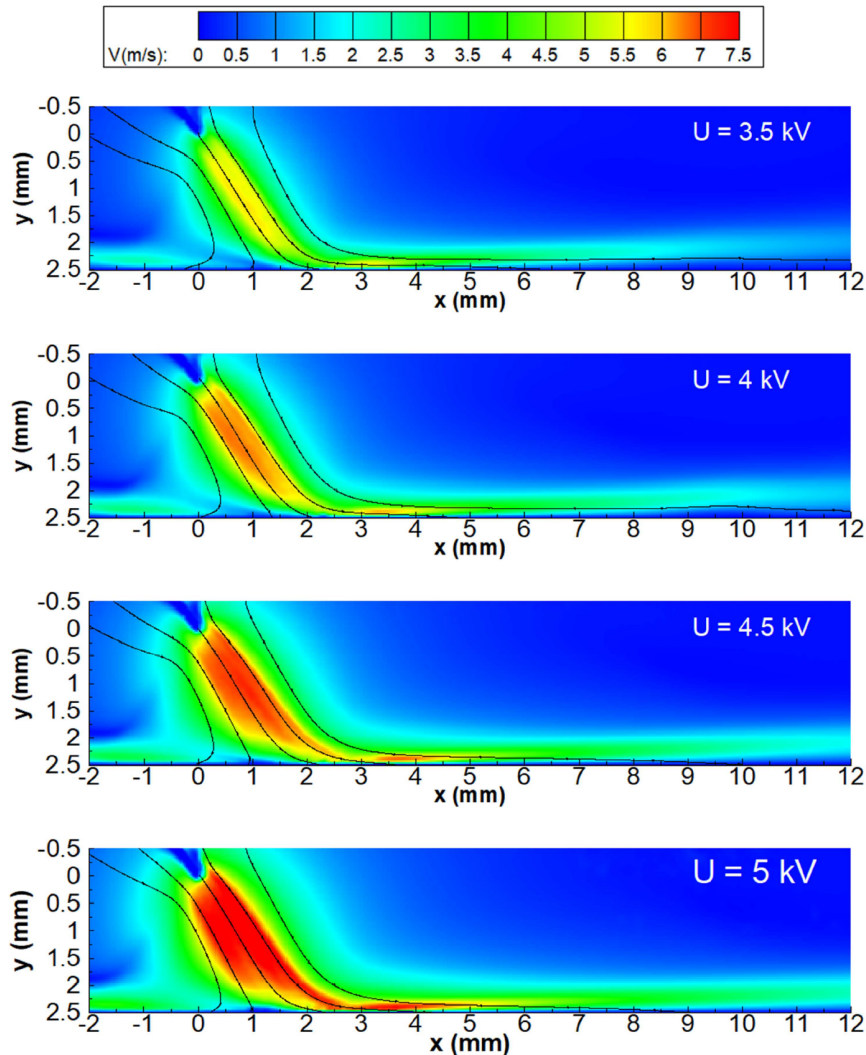


Fig. 8 Velocity fields and streamlines of the ionic wind jet produced by a point-to-plate positive corona discharges with a needle inclined at 45° compared to the plate and a gap of 2.5 mm. The tip is located at (0,0) and the plate at $y = 2.5$ mm.

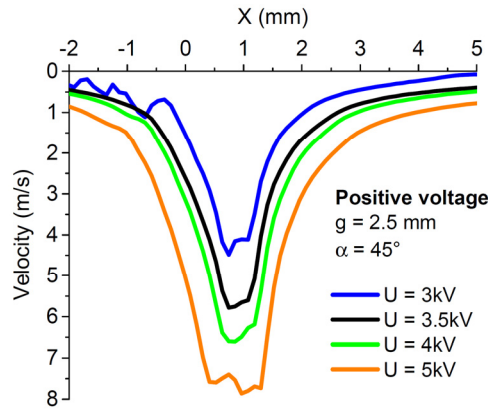


Fig. 9. Velocity profiles of the positive jet along the axis at $y = 1.25$ mm (gap = 2.5 mm and $\alpha = 45^\circ$).

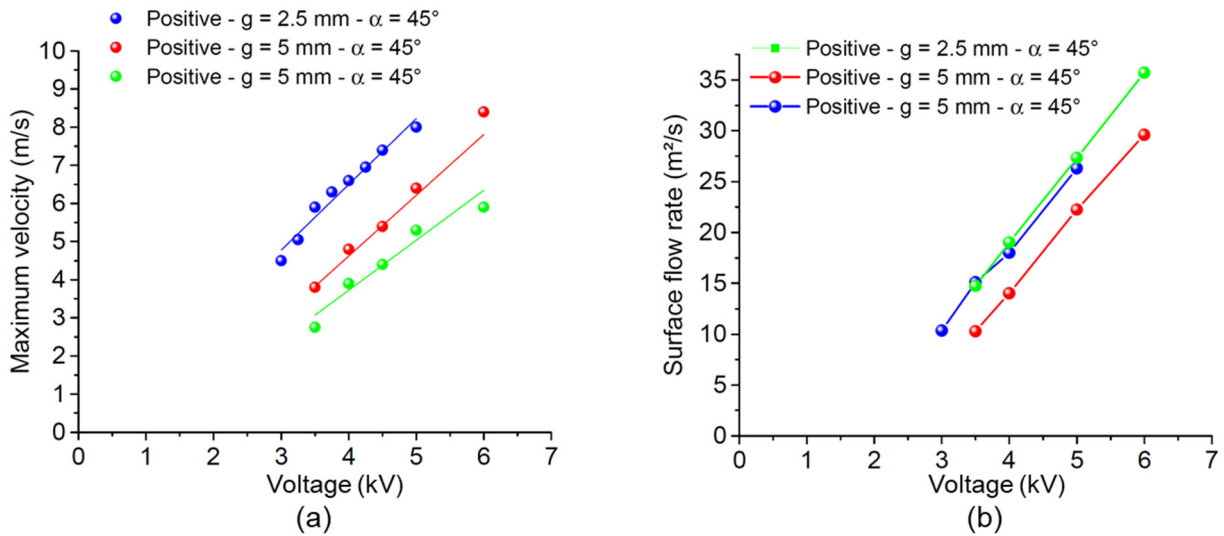


Fig. 10. Maximum velocity (a) and surface flow rate (b) versus applied voltage for three cases: positive corona with a gap equal to 2.5 and 5 mm, and negative corona for a gap of 5 mm.

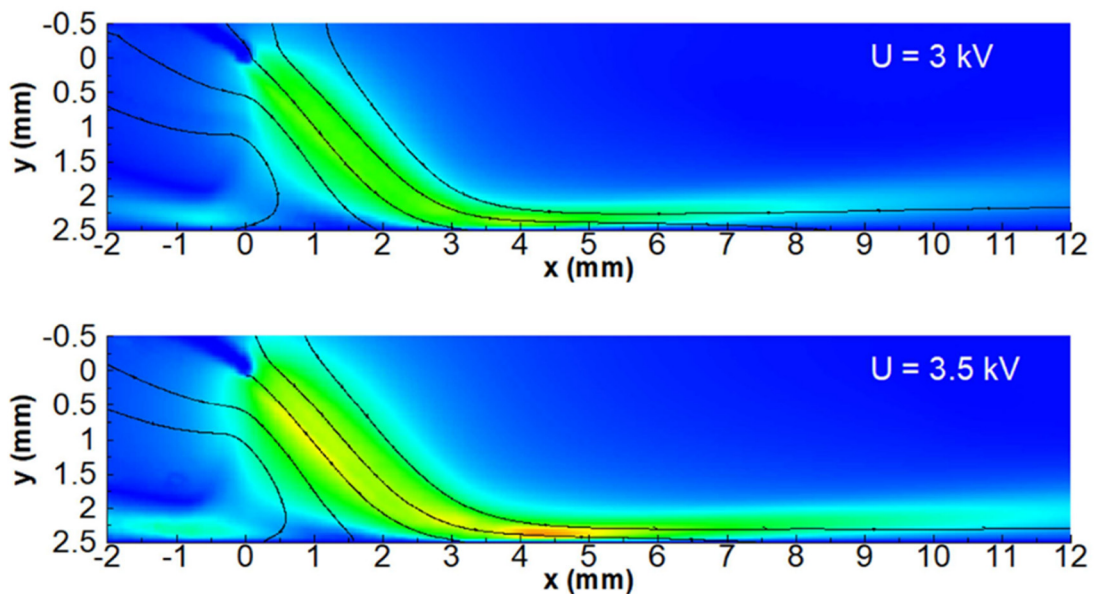


Fig. 11. Velocity fields and streamlines of the ionic wind jet produced by a point-to-plate positive corona discharges with a needle inclined at 30° compared to the plate and a gap of 2.5 mm. The tip is located at (0,0) and the plate at $y = 2.5$ mm.

3.3.3 Influence of the angle α

The objective is here to investigate the effect of the angle on the topology of the ionic wind jet. For that, the angle is reduced to 30° (Fig. 11). As observed previously, the angle jet is still higher than the needle one, 45° instead of 30° in the case of a positive discharge with a gap of 2.5 mm.

3.4 Wall jet study

In this section, we focus on the ionic wind downstream of the stagnation point of the primary jet on the plate electrode. The influence of several input parameters is investigated. The first one is the voltage polarity. Fig. 12 presents velocity profiles in the case of negative and positive corona discharges, for different voltage values ($g = 5$ mm and $\alpha = 45^\circ$), at $x = 6$ mm i.e. about 3.5 mm downstream the impact point. As expected from conservative momentum equation, the positive discharge results in a higher velocity. Moreover, we can see that the height h above the plate wall at which the maximum velocity is obtained is smaller with the positive corona (about $70 \mu\text{m}$ for the positive corona against $250 \mu\text{m}$ for the negative one). This value of $70 \mu\text{m}$ is very interesting as we know that we have to act as close to the wall as possible to be effective in flow control applications.

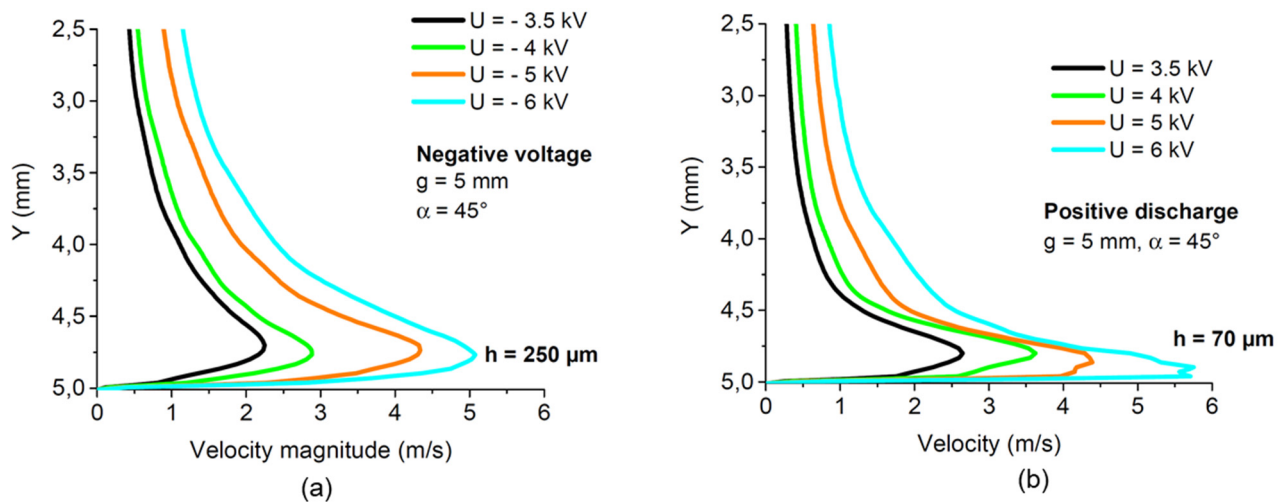


Fig. 12. Velocity profiles along y axis at $x = 6$ mm ($g = 5$ mm and $\alpha = 45^\circ$) for the negative (a) and positive (b) corona discharges.

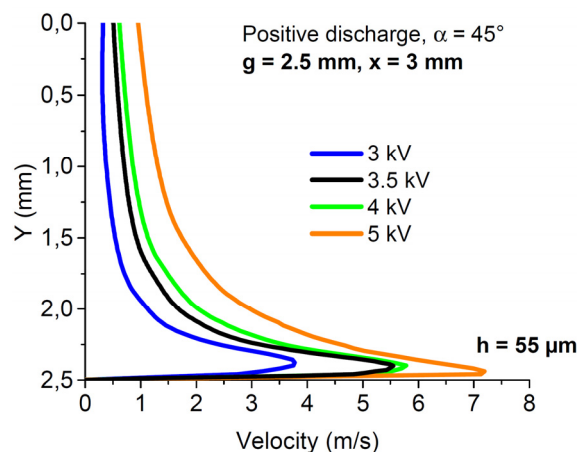


Fig. 13. Velocity profiles along y axis at $x = 3$ mm ($g = 2.5$ mm and $\alpha = 45^\circ$) for the positive corona discharges.

The second parameter is the electrode gap (2.5 and 5 mm). To normalize the distances in x and y , and to be able to compare the wall jet for both gaps, we plotted in Fig.13 the velocity profiles in the case of a positive 2.5-mm-gap corona discharge at $x = 3$ mm (the gap being divided by two, we divided by two the value of x

too). As it can be observed, the velocity is higher and closer to the wall compared to the case with a gap equal to 5 mm (Fig. 12b). Indeed, at 5 kV, the maximum velocity and the height at which it takes place are equal to 7.2 m s^{-1} and $55 \text{ }\mu\text{m}$, respectively, since the maximum velocity with a gap of 5 mm was equal to 4.3 m s^{-1} . However, as highlighted by Fig. 14, this behaviour disappears when x increases. Far from the impact location, at $x = 10 \text{ mm}$ for both gaps, the velocity profiles are surprisingly similar and the height of maximum velocity is close to $300 \text{ }\mu\text{m}$. Finally, the last parameter is the needle angle. In Fig. 15, we plotted the velocity profiles at $x = 10 \text{ mm}$ for both angles (30° and 45°). It is clear that far from the impact location, the weakest angle allows producing the fastest wall jet.

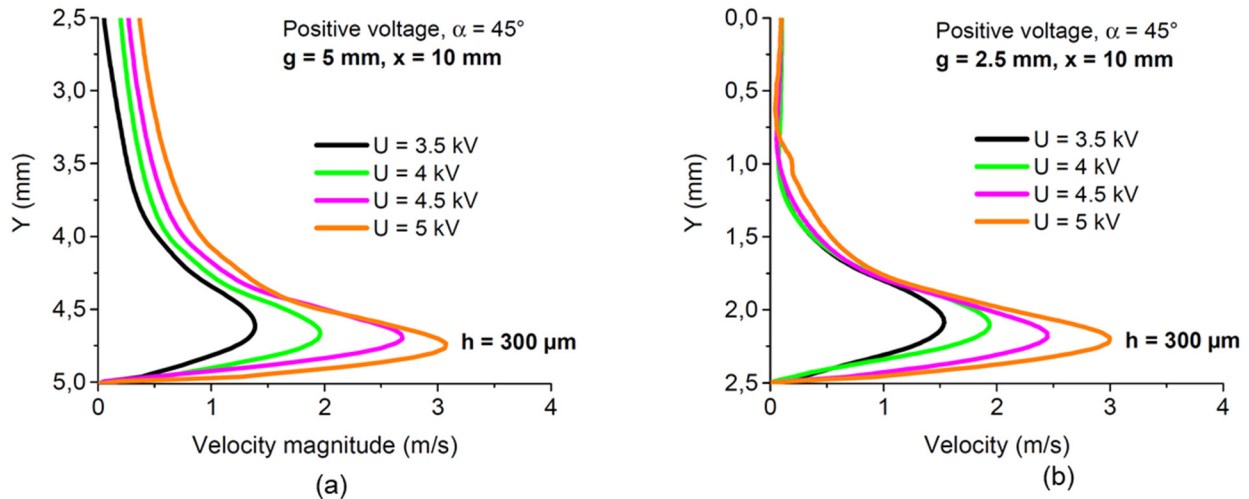


Fig. 14. Velocity profiles along y axis at $x = 10 \text{ mm}$ ($\alpha = 45^\circ$) in the case of the positive corona discharges for two different gaps: (5 mm(a) and 2.5 mm (b)).

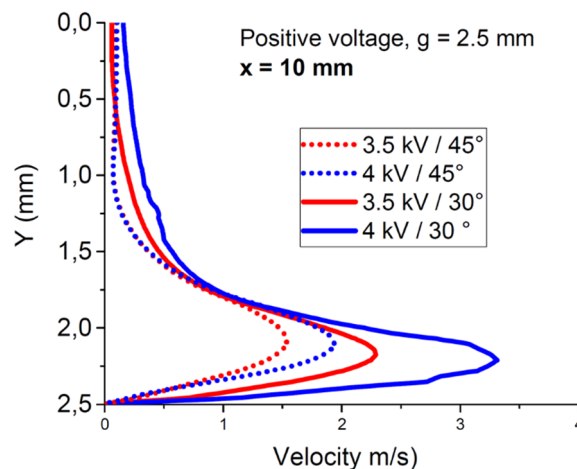


Fig. 15. Velocity profiles along y axis at $x = 10 \text{ mm}$ in the case of the positive corona discharges for two different angles α (30° and 45°). Gap = 2.5 mm.

4. Conclusion

This experimental work aimed at better understanding the electrohydrodynamic phenomena within positive and negative corona discharges with a non-usual geometry: a small gap between both electrodes (down to 2.5 mm) and needle which is not perpendicular to the plate electrode. To our knowledge, when this work has been carried out, only one article of 2017 had studied the ionic wind produced by a positive corona discharge between an inclined needle and a plate [35]. The same research team published a second article on this subject very recently [36], in march 2020.

This work confirmed some results we had already highlighted in the case of a wider gap and a needle perpendicular to the plate [26, 30]: the positive discharge results in a faster ionic wind velocity and the jet that

flows from the tip to the plate is thinner than the one obtained with a negative discharge. Moreover, the velocity fields and associated velocity profiles showed that the topologies of negative and positive jets are fully different. Furthermore, all the measurements realized with the inclined needle reveal new information. First, they highlighted that although the positive discharge generates a faster ionic wind, the negative discharge induces a higher flow rate because the jet width is greater. This is interesting because that shows that, depending on the application, the same polarity will not be used. For ionic wind pumps and blowers, it is more relevant to use a negative voltage (moreover, the velocity is more stable versus time) since for flow control applications, for which the maximum velocity is one of the key parameters, a positive corona discharge seems to be better.

Secondly, we observed that the ionic wind jet depends on the needle angle, such as Elagin *et al* [35]. In fact, the angle of the ionic wind jet is always slightly higher than the needle one (we found angles of 59° and 52° for the negative and positive discharges, respectively, with a needle inclined at 45° and a gap of 5 mm). That highlights a very interesting feature: the electrohydrodynamic force does not occur only close to the tip. Indeed, if it was the case, the force direction would be parallel to the needle (as the electric field lines) and the ionic wind jet too. Then, the small difference between the needle and the jet angles demonstrates that a part of the electrohydrodynamic force that is at the origin of the gas motion takes place in a region where the electric field lines are not parallel to the needle, i.e. far from the tip. By the way, this was visible in Fig. 5b that shows that the maximum ionic wind velocity is not measured close to the tip but at 3 mm far from it, highlighting that there is still a force able to counter the viscous effects at this location.

Finally, the last part of this article was dedicated to the characterization of the wall jet flowing along the plate, downstream the impact of the primary jet starting from the tip. This last study aimed at determining if this type of corona discharge could be used as a plasma actuator in flow control applications, such as surface dielectric barrier discharges (DBD) [22]. Indeed, we can imagine new types of plasma actuators based on a corona discharge established between a set of inclined high voltage needles and the grounded electrode that would be flush mounted on the wall profile. This type of plasma actuators would allow for inducing both effects very suitable: a suction effect toward the wall (depending on the needle angle) and air acceleration very close to the wall, inside the boundary layer. That could be employed for flow separation control in aerodynamics applications or for enhancing thermal exchanges at an air-solid wall. The results are encouraging since velocities comparable to those produced by DBD have been measured in the present study, and it seems that the maximum velocity is located closer to the wall compared to DBD.

Acknowledgment

This work has been funded by the French Government program INVESTISSEMENT D'AVENIR (LABEX INTERACTIFS, reference ANR-11-LABX-0017-01).

References

- [1] Moreau, E. and Touchard, G., Enhancing the mechanical efficiency of electric wind in corona discharges, *J. Electrostat.*, Vol. 66, pp. 39–44, 2008.
- [2] Robinson, M., Movement of air in the electric wind of the corona discharge, *Trans. Am. Inst. Electr. Eng. Part Commun. Electron.*, Vol. 80, pp. 143–150, 1961.
- [3] Tsubone, H., Ueno, J., Komeili, B., Minami, S., Harvel G.D., Urashima, K., Ching, C.Y., and Chang, J.S., Flow characteristics of dc wire-non-parallel plate electrohydrodynamic gas pumps, *J. Electrostat.* Vol. 66, pp. 115–121, 2008.
- [4] June, M. S., Kribs, J., and Lyons, K. M., Measuring efficiency of positive and negative ionic wind devices for comparison to fans and blowers, *J. Electrostat.*, Vol. 69, pp. 345–350, 2011.
- [5] Kim, C., Park, D., Noh, K. C., and Hwang, J., Velocity and energy conversion efficiency characteristics of ionic wind generator in a multistage configuration, *J. Electrostat.*, Vol. 68, pp. 36–41, 2010.
- [6] Rickard, M., Dunn-Rankin, D., Weinberg, F., and Carleton, F., Maximizing ion-driven gas flows, *J. Electrostat.*, Vol. 64, pp. 368–376, 2006.
- [7] Mizuno, A., Electrostatic precipitation, *IEEE Trans. Dielectr. Electr. Insul.*, Vol. 7, pp. 615–624, 2000.
- [8] Dramane, B., Zouzou, N., Moreau, E. and Touchard, G., Electrostatic precipitation in wire-to-cylinder configuration: Effect of the high-voltage power supply waveform, *J. Electrostat.*, Vol. 67, pp.117–122, 2009.
- [9] Dramane, B., Zouzou, N., Moreau, E. and Touchard, G., Electrostatic precipitation of submicron particles using a DBD in axisymmetric and planar configurations, *IEEE Trans. Dielectr. Electr. Insul.*, Vol. 16, pp.343–351, 2009.

- [10] Huang, Y., Li, S., Zheng, Q., Shen, X., Wang, S., Han, P., Liu, Z., and Yan, K., Recent progress of dry electrostatic precipitation for PM 2.5 emission control from coal-fired boilers, *Int. J. Plasma Environ. Sci. Technol.*, Vol. 9 (2), pp. 69–95, 2015.
- [11] Souakri, S., Reess, T., Silvestre De Ferron, A., F. Lemont, F., and Marchand, M., Flue gas treatment by ESP: realization and optimization of an emissive electrode., *Int. J. Plasma Environ. Sci. Technol.*, Vol. 10 (2), pp. 173–180, 2016.
- [12] Lai, F. C., Huang, M. and Wong, D. S., EHD-enhanced water evaporation, *Dry. Technol.*, Vol. 22 (3), pp. 597–608, 2004.
- [13] Bajgai, T. R., and Hashinaga, F., Drying of spinach with a high electric field, *Dry. Technol.*, Vol. 19 (9), pp. 2331–2341, 2001.
- [14] Cao, W., Nishiyama, Y., and Koide, S., Electrohydrodynamic drying characteristics of wheat using high voltage electrostatic field., *J. Food Eng.*, Vol. 62, pp. 209–213, 2004.
- [15] Ong, A. O., Abramson, A. R. and Tien, N. C., Optimized and microfabricated ionic wind pump array as a next generation solution for electronics cooling systems. in *13th InterSociety Conference on Thermal and Thermomechanical Phenomena in Electronic Systems*, pp. 1306–1311, 2012. doi:10.1109/ITHERM.2012.6231571.
- [16] Yang, F., Jewell-Larsen, N.E., Brown, D.L., Pendergrass, K., Parker, D.A., Krichtafovitch, I.A., and Mamishev, A.V., Corona driven air propulsion for cooling of electronics, *XIIIth International Symposium on High Voltage Engineering*, Netherlands, 2003.
- [17] Audier, P., Fénot, M., Bénard, N., and Moreau, E., Film cooling effectiveness enhancement using surface dielectric barrier discharge plasma actuator, *Int. J. Heat Fluid Flow*, Vol. 62, pp. 247–257, 2016.
- [18] Audier, P., Fénot, M., Bénard, N., and Moreau, E., Flow control of an elongated jet in cross-flow: Film cooling effectiveness enhancement using surface dielectric barrier discharge plasma actuator, *Appl. Phys. Lett.*, Vol. 108 (8), pp. 084103, 2016.
- [19] Wang, J., Zhu, T., Cai, Y., Zhang, J., and Wang, J. Review on the recent development of corona wind and its application in heat transfer enhancement, *Int. J. Heat Mass Transf.*, Vol. 152, pp. 119545, 2020.
- [20] Ryu, J., Wakida, T., and Takagishi, T., Effect of corona discharge on the surface of wool and its application to printing, *Text. Res. J.*, Vol. 61 (10), pp. 595–601, 1991.
- [21] Moreau, E., Airflow control by non-thermal plasma actuators, *J. Phys. D: Appl. Phys.*, Vol. 40 (3), pp. 605–636, 2007.
- [22] Benard, N., and Moreau, E., Electrical and mechanical characteristics of surface AC dielectric barrier discharge plasma actuators applied to airflow control, *Exp. Fluids*, Vol. 55, pp. 1846, 2014.
- [23] Gilmore, C. K. and Barrett, S. R. H., Electroaerodynamic thruster performance as a function of altitude and flight speed, *AIAA J.*, Vol. 56, pp. 1105–1117, 2018.
- [24] Wilson, J., Perkins, H. D., and Thompson, W. K., An Investigation of ionic wind propulsion. *NASA/TM—2009-215822*, 2009.
- [25] Moreau, E., Benard, N., Lan-Sun-Luk, J.-D., and Chabriat, J.-P., Electrohydrodynamic force produced by a wire-to-cylinder dc corona discharge in air at atmospheric pressure, *J. Phys. D: Appl. Phys.*, Vol. 46 (47), pp. 475204, 2013.
- [26] Moreau, E., Audier, P., and Benard, N., Ionic wind produced by positive and negative corona discharges in air, *J. Electrostat.*, Vol. 93, pp. 85–96, 2018.
- [27] Moreau, E., Audier, P., Orriere, T., and Benard, N. Electrohydrodynamic gas flow in a positive corona discharge, *J. Appl. Phys.*, Vol. 125, pp. 133303, 2019.
- [28] Johnson, M. J., and Go, D. B., Recent advances in electrohydrodynamic pumps operated by ionic winds: a Review, *Plasma Sources Sci. Technol.*, Vol. 26 (10), pp. 103002, 2017.
- [29] Mizeraczyk, J., Berendt, A. and Podlinski, J., Temporal and spatial evolution of EHD particle flow onset in air in a needle-to-plate negative DC corona discharge, *J. Phys. D: Appl. Phys.*, Vol. 49 (20), pp. 205203, 2016.
- [30] Defoort, E., Bellanger, R., Batiot-Dupeyrat, C., and Moreau, E., Ionic wind produced by a DC needle-to-plate corona discharge with a gap of 15 mm., *J. Phys. D: Appl. Phys.*, Vol. 53 (17), pp. 175202, 2020.
- [31] Fylladitakis, E. D., Theodoridis, M. P., and Moronis, A. X., Review on the history, research, and applications of electrohydrodynamics, *IEEE Trans. Plasma Sci.*, Vol. 42 (2), pp. 358–375, 2014.
- [32] *Philosophia Magnetica* by Niccolo Cabeo - AbeBooks. <https://www.abebooks.com/booksearch/title/philosophiamagnetica/author/niccolo-cabeo/>.
- [33] Opticks: or, A treatise of the reflections, refractions, inflexions and colours of light. Also two treatises of the species and magnitude of curvilinear figures: Newton, Isaac, Sir, 1642-1727: Free Download, Borrow, and Streaming: Internet Archive. <https://archive.org/details/opticksortreatis00newt/page/24>.
- [34] Chattock, A. P. XLIV. On the velocity and mass of the ions in the electric wind in air. *Lond. Edinb. Dublin Philos. Mag. J. Sci.*, Vol. 48, pp. 401–420, 1899.
- [35] Elagin, I. A., Begal', D. I., Ashikhmin, I. A. and Stishkov, Y. K., Change in the direction of electric wind from a wire electrode tilted relative to a grounded plane, *Tech. Phys. Lett.*, Vol. 43, pp. 98–100, 2017.
- [36] Elagin, I., Samusenko, A. and Chirkov, V. Numerical study of the needle inclination angle effect on the ionic wind

- direction, *Int. J. Plasma Environ. Sci. Technol.*, Vol. 14 (1), pp. e01006, 2020.
- [37] Zouzou, N., Moreau, E. and Touchard, G. Précipitation électrostatique dans une configuration pointeplan, *J. Electrostat.*, Vol. 64, pp. 537–542, 2006.
- [38] Defoort, E., Moreau, E., Batiot-Dupeyrat, C., and Bellanger, R., Electrodynamic airflow produced by a point-to-plate DBD plasma reactor in presence of a water mist, *International Symposium on ElectroHydroDynamics (ISEHD 2019)*, St Petersburg, Russia, 18–22 June, 2019.
- [39] Moreau, E., and Benard, N., Ionic wind produced by positive and negative DC point-to-plate corona discharges in air, *11th International Symposium on Non-Thermal/Thermal Plasma Pollution Control Technology & Sustainable Energy*, Padova, Italy, July 2–5, 2018.
- [40] Akishev, Y. S., Aponin G.I., Grushin, M. G., Karalnik, V. B., Petryakov, A.V., and Trushkin N.I., Determination of local ionic wind velocity in corona by laser interferometer taking into consideration the charging–discharging of probe particles, *IEEE Trans. Plasma Sci.*, Vol. 37 (6), pp. 1034–1044, 2009.
- [41] Drews, A. M., Cademartiri, L., Whitesides, G. M., and Bishop, K. J. M., Electric winds driven by time oscillating corona discharges, *J. Appl. Phys.*, Vol. 114, pp. 143302, 2013.